doi:10.1016/j.ymthe.2006.08.009

ARTICLE

Autophagy and Mistargeting of Therapeutic Enzyme in Skeletal Muscle in Pompe Disease

Tokiko Fukuda,[1] Meghan Ahearn,[1] Ashley Roberts,[1] Robert J. Mattaliano,[2] Kristien Zaal,[3] Evelyn Ralston,[3] Paul H. Plotz,[1] and Nina Raben[1,*]

[1]*Arthritis and Rheumatism Branch and* [3]*Light Imaging Section, Office of Science and Technology, National Institute of Arthritis and Musculoskeletal and Skin Diseases, National Institutes of Health, Bethesda, MD 20892, USA*
[2]*Cell and Protein Therapeutics R&D, Genzyme Corporation, Framingham, MA 01701, USA*

**To whom correspondence and reprint requests should be addressed at 9000 Rockville Pike, Clinical Center Building 10/9N244, NIH, NIAMS, Bethesda, MD 20892-1820, USA. Fax: +1 301 402 0012. E-mail: rabenn@arb.niams.nih.gov.*

Enzyme replacement therapy (ERT) became a reality for patients with Pompe disease, a fatal cardiomyopathy and skeletal muscle myopathy caused by a deficiency of glycogen-degrading lysosomal enzyme acid α-glucosidase (GAA). The therapy, which relies on receptor-mediated endocytosis of recombinant human GAA (rhGAA), appears to be effective in cardiac muscle, but less so in skeletal muscle. We have previously shown a profound disturbance of the lysosomal degradative pathway (autophagy) in therapy-resistant muscle of GAA knockout mice (KO). Our findings here demonstrate a progressive age-dependent autophagic buildup in addition to enlargement of glycogen-filled lysosomes in multiple muscle groups in the KO. Trafficking and processing of the therapeutic enzyme along the endocytic pathway appear to be affected by the autophagy. Confocal microscopy of live single muscle fibers exposed to fluorescently labeled rhGAA indicates that a significant portion of the endocytosed enzyme in the KO was trapped as a partially processed form in the autophagic areas instead of reaching its target—the lysosomes. A fluid-phase endocytic marker was similarly mistargeted and accumulated in vesicular structures within the autophagic areas. These findings may explain why ERT often falls short of reversing the disease process and point toward new avenues for the development of pharmacological intervention.

Key Words: acid α-glucosidase, lysosome, autophagy, live cultured myofibers, glycogen storage, endocytosis, enzyme replacement therapy, lipofuscin

Introduction

Enzyme replacement therapy (ERT) has been successfully applied for a number of lysosomal storage disorders [1] and is now available for patients with Pompe disease (glycogen storage disease type II), an inherited deficiency of acid α-glucosidase (GAA), the lysosomal enzyme responsible for the breakdown of glycogen to glucose. Glycogen delivery to the lysosomes is still poorly understood, but is thought to occur through autophagocytosis. The GAA deficiency results in intralysosomal accumulation of glycogen in multiple tissues, with skeletal and cardiac muscles being most affected clinically. The disease phenotype ranges from the most severe infantile variant to an indolent late-onset form [2]. The infantile form is characterized by cardiomegaly, progressive skeletal muscle weakness, and death within the first year of life in the majority of patients [3,4]. Late-onset forms manifest as slow progressive skeletal muscle disease with respiratory muscle involvement but without cardiac involvement [5,6].

The concept of ERT for Pompe disease and many lysosomal storage disorders is based on extensive experimental evidence indicating that lysosomal enzymes can be taken up by the cells through receptor-mediated endocytosis. Cation-independent mannose 6-phosphate receptor (CI-MPR) on the cell surface binds lysosomal enzymes that are tagged with a mannose 6-phosphate (M6P) recognition marker, directing the enzymes into the endocytic pathway. The receptor–enzyme complex enters the cells in clathrin-coated vesicles that fuse with early endosomes, which in turn fuse with late endosomes. The acidic pH of late endosomes induces the dissociation of the complex; the enzyme is subsequently packaged into the lysosome, and the receptor is recycled [7,8]. Numerous proteins participate in the sorting and trafficking of the lysosomal enzymes (reviewed in [9]). The same endocytic pathway delivers endogenous lysosomal enzymes to the lysosomal compartment. In Pompe disease, the recombinant enzyme is a 110-kDa precursor containing N-linked oligosaccharide chains modified with M6P residues that enable the enzymes to bind the receptor.

1525-0016/$30.00

ARTICLE
doi:10.1016/j.ymthe.2006.08.009

Like the 110-kDa endogenous GAA precursor, the recombinant human GAA (rhGAA) is expected to undergo sequential proteolytical cleavage along the transport route to yield intermediate forms followed by conversion to the fully active mature lysosomal species [10,11].

Both clinical trials and our preclinical studies have indicated that ERT is effective in glycogen clearance in cardiac muscle, but reversal of pathology in skeletal muscle has not always been achieved [12–18]. Furthermore, there is a differential response to ERT in type I and type II fibers in GAA knockout (KO) mice. Type II fibers, which showed strikingly enhanced autophagy in comparison to type I fibers, have proven resistant to therapy [18,19]. Autophagy, a lysosomal-dependent process, is a conserved mechanism of degradation of long-lived proteins and damaged organelles. Double membrane-bound autophagosomes deliver cytoplasmic constituents destined for degradation to the late endosomes and lysosomes, the sites where the endocytic and autophagic pathways converge (reviewed in [20–22]). We now demonstrate that there is a progressive age-dependent autophagic buildup in KO muscle fibers and that this buildup has a profound effect on therapy as it diverts the recombinant enzyme from the lysosomes, the site of glycogen accumulation.

RESULTS

Age-Dependent Autophagic Buildup in ERT-Resistant Type II Fibers in KO Mice

We have previously demonstrated massive autophagic buildup in muscle fibers isolated from type II-rich gastro-

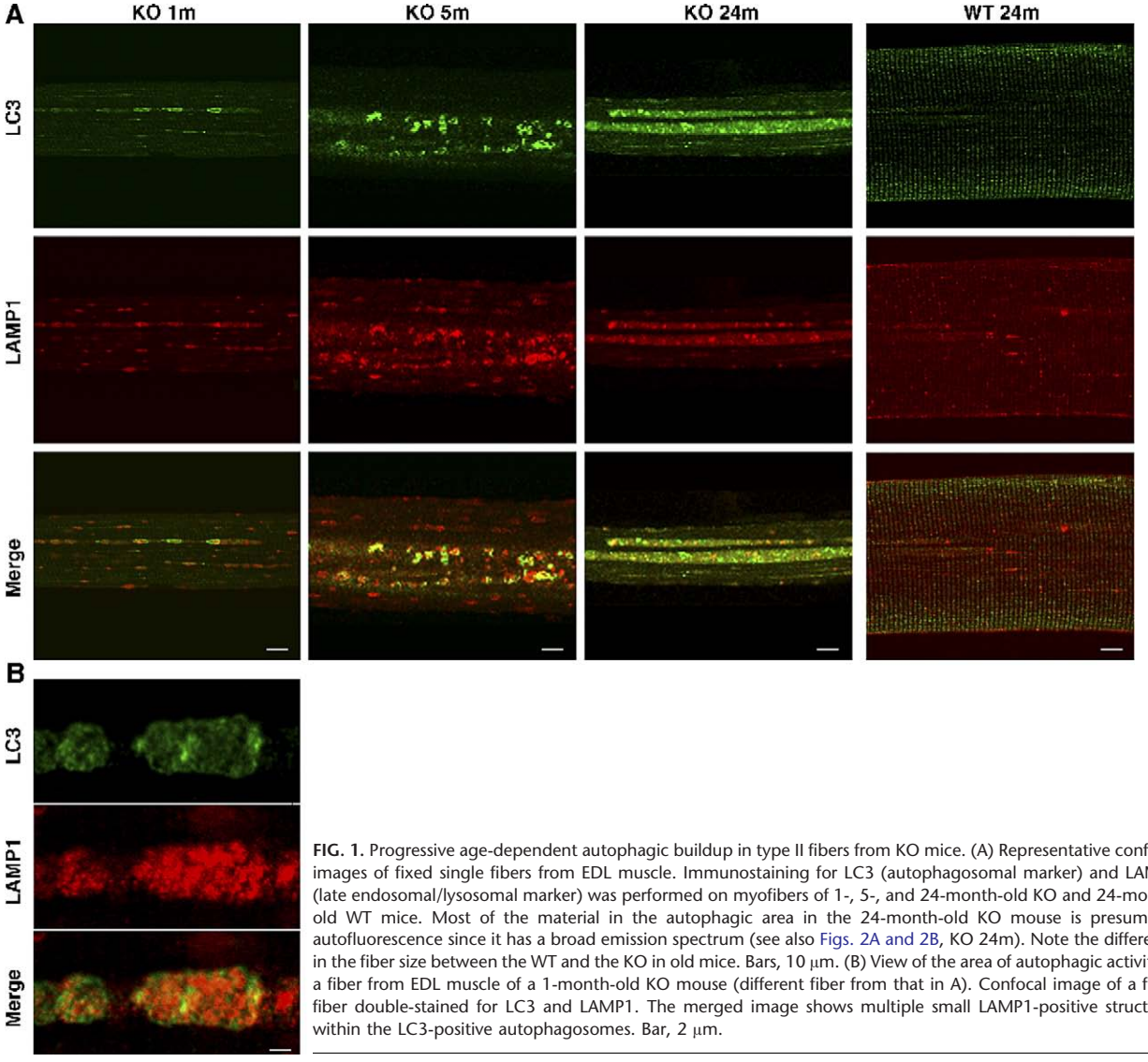

FIG. 1. Progressive age-dependent autophagic buildup in type II fibers from KO mice. (A) Representative confocal images of fixed single fibers from EDL muscle. Immunostaining for LC3 (autophagosomal marker) and LAMP1 (late endosomal/lysosomal marker) was performed on myofibers of 1-, 5-, and 24-month-old KO and 24-month-old WT mice. Most of the material in the autophagic area in the 24-month-old KO mouse is presumably autofluorescence since it has a broad emission spectrum (see also Figs. 2A and 2B, KO 24m). Note the difference in the fiber size between the WT and the KO in old mice. Bars, 10 μm. (B) View of the area of autophagic activity in a fiber from EDL muscle of a 1-month-old KO mouse (different fiber from that in A). Confocal image of a fixed fiber double-stained for LC3 and LAMP1. The merged image shows multiple small LAMP1-positive structures within the LC3-positive autophagosomes. Bar, 2 μm.

doi:10.1016/j.ymthe.2006.08.009

cnemius (G) muscle but not from type I-rich soleus muscle of aged GAA KO mice (8–10 months of age) [19]. To study the age-related changes in autophagy in multiple type II muscle groups, we analyzed single muscle fibers from extensor digitorum longus (EDL), tibialis anterior (TA), and white gastrocnemius muscles from 1- to 24-month-old KO mice.

Confocal microscopy of fixed myofibers immunostained with a highly specific autophagosomal marker, LC3, and a late endosomal/lysosomal marker, lysosomal-

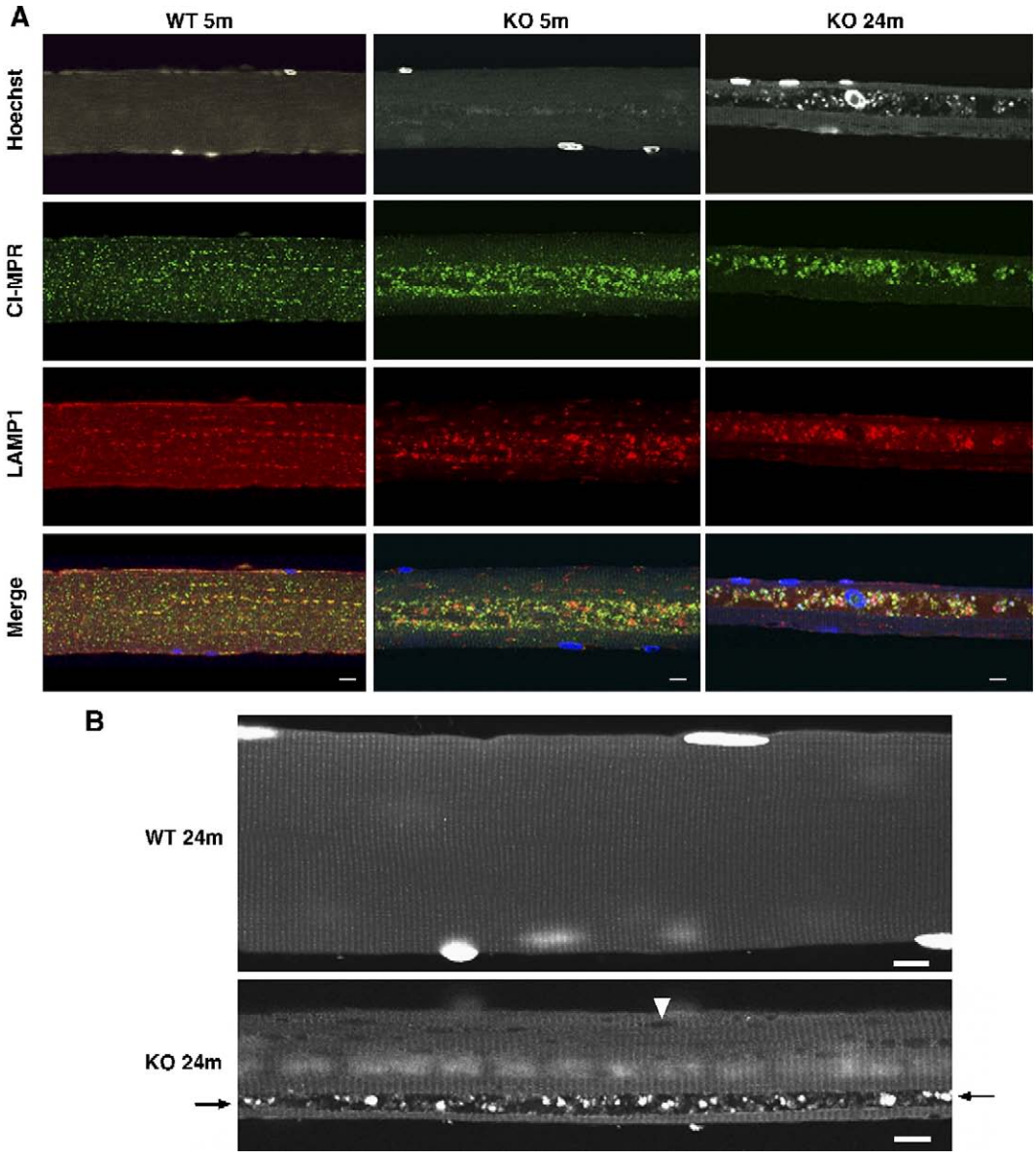

FIG. 2. CI-MPR- and LAMP1-positive structures in autophagic areas in KO mice. (A) Representative confocal images of fixed single fibers from EDL muscle. Immunostaining for CI-MPR (negative marker for lysosomes) and LAMP1 was performed on myofibers from WT (shown for 5-month-old) and KO mice. Nuclei were stained with Hoechst. CI-MPR staining in WT fibers appears as small dot-like structures often overlapping or in close proximity to LAMP1-positive structures. In fibers from a 5-month-old KO mouse the receptor is abundant in the autophagic area. In fibers from a 24-month-old KO mouse most of the structures within the autophagic areas are autofluorescence with a broad emission spectrum as evidenced by a similar pattern produced by any of the three excitation lasers (405, 488, and 543 nm). (B) Accumulation of autofluorescent materials in autophagic area from a 24-month-old KO mouse. Note the difference in fiber size between WT and KO. Confocal images of EDL fibers stained with Hoechst were taken using 405-nm excitation. The autophagic area, which interrupts muscle striations in the KO fiber, is located toward the periphery of this particular fiber (KO 24m). Bright structures with irregular shape are autofluorescent material in the KO mouse (arrows). Small dark structures (arrowhead) outside the autophagic area are most likely swollen lysosomes. Nuclei, out of focus in this single optical section, appear as a chain in the center of the KO fiber. Bars, 10 μm.

ARTICLE
doi:10.1016/j.ymthe.2006.08.009

associated membrane protein 1 (LAMP1), revealed clusters of LC3-positive vesicles in KO fibers from all muscle groups examined; the increased autophagy was already detectable at 1 month of age in the KO mice (Figs. 1A and 1B shown for EDL). The centrally localized regions of autophagic activity in fibers from young 1-month-old animals occupied a small segment (30–90 μm in length) of the fiber (Fig. 1A). These regions contained clusters of tiny LAMP1-positive structures (some smaller than those outside the autophagic area), typically without clear membrane boundaries, and a number of LC3-positive autophagosomes. These LAMP1-positive structures were often found within the distinctly LC3-positive autophagosomes (Fig. 1B).

Autophagy increased with age in the KO mice. In 5-month-old KO mice, the autophagic buildup, found in every fiber, extended over most of the length of the fibers and contained multiple LC3- and LAMP1-positive vesicles, as well as LC3/LAMP1 double-positive vesicles (Fig. 1A). In 24-month-old KO mice, the autophagic area was strikingly large relative to the size of the fiber. In some fibers, the diameter of the autophagic areas was greater than half the diameter of the fiber itself. Moreover, there seemed to be fewer vesicles within the area compared to younger mice, and we found multiple deposits of autofluorescent material (Figs. 1A and 2). In contrast to the KO mice, autophagy was not detectable in fibers from WT mice of any age (shown in Fig. 1A for a 24-month-old mouse). Thus, age-dependent autophagic buildup in the KO is due to the progressive nature of the disease rather than the result of normal aging.

The autophagic areas in 5-month-old KO mice had intense CI-MPR staining and contained multiple late endosomes, as shown by the presence of LAMP1/CI-MPR double-positive vesicles (the receptor is present on late endosomes but not on lysosomes) (Fig. 2A). Fusion of late endosomes and autophagosomes in the autophagic areas may explain the presence of the LC3/LAMP1 double-positive vesicles (intermediate autophagosomes or amphisomes) described above. Alternatively, these LC3/LAMP1 double-positive vesicles may be a product of fusion of autophagosomes and dysfunctional lysosomes that are unable to digest the autophagosomal membrane protein LC3.

The autophagic areas in 24-month-old KO mice had intense signal when stained for CI-MPR. However, the pattern of staining differed from that observed in the 5-month-old KO, in that most of the signal had a broad emission spectrum suggesting the presence of undigested autofluorescent material (Figs. 2A and 2B, KO shown with Hoechst). Additionally, there were fewer LAMP1-positive/CI-MPR-negative structures in the autophagic areas compared to younger KO mice, suggesting that the number of intact lysosomes was reduced with age (CI-MPR is a negative marker for lysosomes). Some of the autofluorescent material was contained within the lyso-

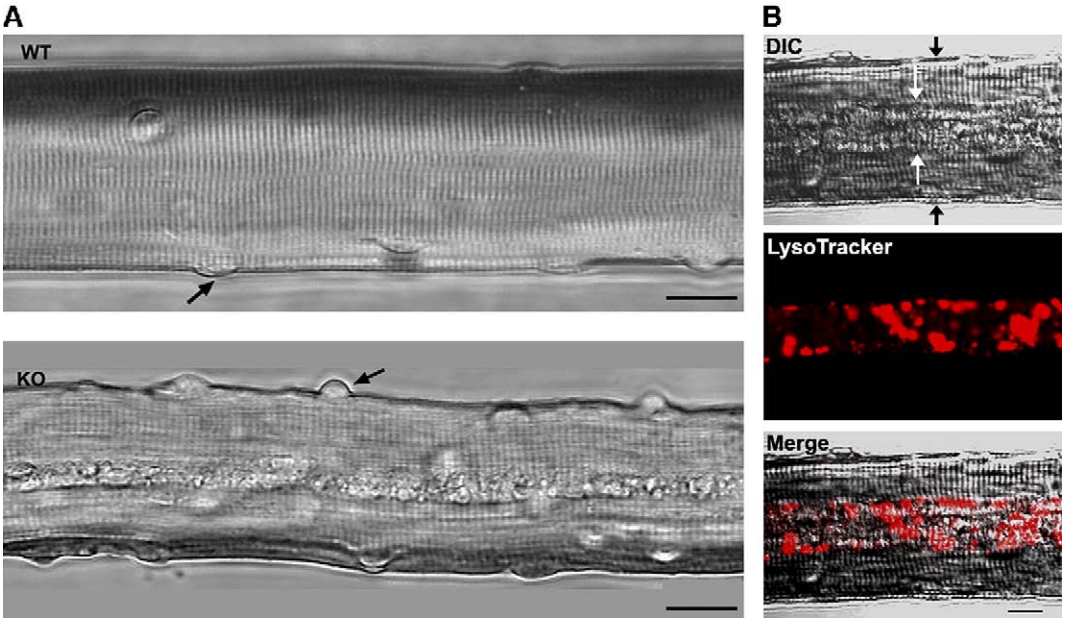

FIG. 3. Vesicular structure of the autophagic areas. (A) Multiple vesicles could be observed in live KO fibers by transmitted light microscopy in the core of the fiber. Live gastrocnemius fibers with satellite cells (arrows) from 2-month-old WT and KO mice are shown. Bars, 20 μm. (B) Confocal image of a live fiber (G of a 3-month-old KO mouse) incubated for 30 min with LysoTracker (75 nM), showing multiple acidic vesicles in the autophagic area. Black arrows point to the margins of the fiber, and white arrows point to the autophagic area in the core of the fiber on the DIC (differential interference contrast) image. Note that LysoTracker is not visible outside the autophagic area because the detection gain was adjusted to avoid saturation in the autophagic area. Bar, 10 μm.

doi:10.1016/j.ymthe.2006.08.009

somes (lipofuscin), while some appeared to be outside the lysosomes. There was no significant difference in the distribution of the CI-MPR and LAMP1 in 24-month-old WT mice (not shown) compared to the 5-month-old WT (Fig. 2A).

Endocytosis of rhGAA in Live Cultured Type II Fibers in KO

It seemed reasonable to assume that the autophagic buildup and the changes in the distribution of the CI-MPR may affect the trafficking of the therapeutic enzyme. Therefore, we analyzed the endocytosis of rhGAA in live cultured type II fibers from the KO mice. We isolated viable single fibers with their satellite cells, surrounded by a basal lamina but free of connective tissues, blood vessels, and nerves, from 2- to 3-month-old mice. The huge, centrally localized autophagic areas were clearly seen without staining by low-resolution transmitted light microscopy (Fig. 3A shown for gastrocnemius). The acidic nature of the vesicular structures within the autophagic areas was confirmed by labeling live fibers with LysoTracker, which selectively accumulates in vesicles with low pH (Fig. 3B).

We exposed KO and WT live fibers to fluorescently labeled rhGAA (Alexa Fluor 546-rhGAA) for 16–20 h, extensively washed them, and analyzed them by confocal microscopy (Figs. 4A and 4B). In live WT fibers the distribution pattern of the labeled enzyme was similar to that observed in fixed fibers stained with LAMP1 (Fig. 4B; see Figs. 1A and 2A WT for typical LAMP1 staining pattern), strongly suggesting that the labeled enzyme reached lysosomes. When we incubated live KO fibers with labeled rhGAA, a significant amount of the enzyme ended up in the vesicular structures within autophagic areas (Fig. 4A). Similarly, Alexa Fluor 546-conjugated dextran, a fluid-phase endocytic marker, accumulated primarily in the autophagic areas (Fig. 4C). The endocytosis of the labeled enzyme was significantly inhibited when the fibers were exposed to either mannose 6-phosphate or unlabeled rhGAA prior to incubation with

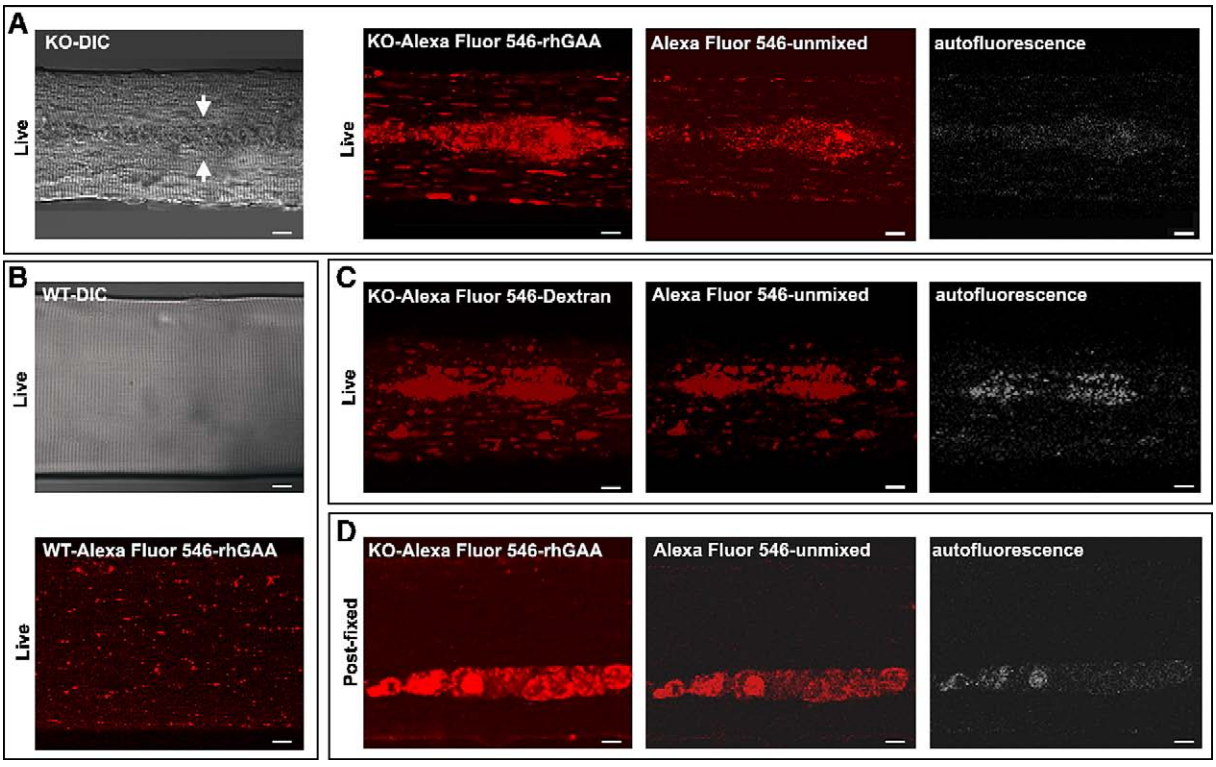

FIG. 4. Detection of the endocytosed fluorescently labeled rhGAA and dextran in autophagic area. (A) Confocal images showing the distribution of the labeled enzyme in a live fiber from EDL of a 3-month-old KO mouse. Labeled rhGAA is concentrated in the autophagic area, which is marked by arrows in the DIC image. The two images on the left were taken by channel mode. The contribution of autofluorescence was evaluated by separation of Alexa Fluor 546-specific emission signal from the autofluorescence with a spectral detector (λ mode) and linear unmixing analysis. (B) Confocal images showing the distribution of the labeled enzyme in a live fiber from EDL muscle of a 3-month-old WT mouse. The images were taken by channel mode. (C) Confocal images showing the distribution of Alexa Fluor 546-conjugated dextran and contribution of autofluorescence in a live KO fiber from EDL of a 3-month-old mouse. (D) Confocal images showing the distribution of the labeled enzyme and contribution of autofluorescence in a fiber from G muscle of a 3-month-old KO mouse. Unlike the image in (A), the live fiber was first labeled with Alexa Fluor 546-rhGAA and then fixed. The images on the left in (C) and (D) were taken by channel mode. Bars, 10 μm.

ARTICLE

doi:10.1016/j.ymthe.2006.08.009

the labeled enzyme (the signal was detected in less than 10 and 20% of fibers, respectively; not shown), suggesting that the enzyme entered the cell mainly through MPR-mediated endocytosis and that the properties of the labeled and unlabeled forms of the enzyme are similar.

To rule out the possibility that autofluorescence is the source of the emission signal observed in the rhGAA-labeled live fibers, we used spectral analysis of the images to separate the Alexa Fluor 546 signal (see Materials and Methods). The signal from the labeled enzyme remained strong in the autophagic areas after linear unmixing of the images even though autofluorescence contributed to the intensity of the initial signal (Fig. 4A). We obtained similar results when we performed linear unmixing for experiments with Alexa Fluor 546-conjugated dextran (Fig. 4C).

Since the labeled rhGAA still contained a small amount (<10%) of free dye as detected by thin-layer chromatography (TLC), we incubated the fibers with the dye alone. After linear unmixing, no Alexa Fluor 546-specific signal was detected in live or postfixed fibers (not shown). In contrast, in the postfixed KO fibers incubated with the labeled enzyme (the labeled protein is expected to persist after fixation) a strong signal was still detected in the autophagic areas (Fig. 4D). Together, these data indicate that much of the endocytosed recombinant enzyme is trapped in the autophagic areas in KO fibers.

Processing of rhGAA in Myofibers from KO

The accumulation of rhGAA in the autophagic area prompted us to look at the processing of the enzyme in myofibers. We also compared the levels of rhGAA in isolated muscle fibers to those in whole muscle tissue in mice on ERT. For these experiments we administered unlabeled rhGAA either as a single dose or as multiple injections into KO mice. We isolated both tissue and fibers from EDL, TA, and G muscles from each mouse. We compared lysates from whole muscle tissue and fibers from each muscle group by Western analysis. As expected, in all muscle tissues, the predominant species was the 76-kDa mature lysosomal form, and the 95-kDa intermediate was a minor product (shown for G in Fig. 5). Unexpectedly, the level of the mature 76-kDa form in KO myofibers (F in Fig. 5) from each muscle group was significantly less than that from the tissue lysates (T in Fig. 5). This is in contrast to WT, in which the level of endogenous enzyme is equal in both tissues and myofibers. Furthermore, in the KO fibers, the 95-kDa intermediate was significantly increased relative to the mature lysosomal form, indicating that the rhGAA was not completely processed in KO myofibers.

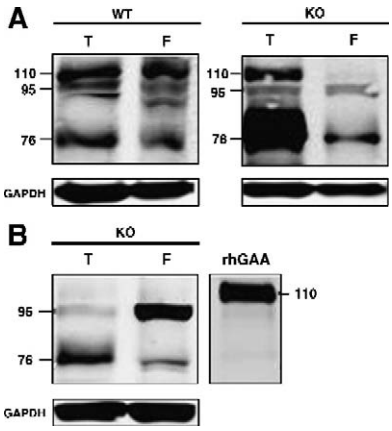

FIG. 5. Detection of administered unlabeled rhGAA in whole muscle tissues and fibers. Western blots showing the levels of endogenous GAA in WT and the level of rhGAA in KO mice after ERT (shown for gastrocnemius muscle). T, whole muscle tissue; F, fibers. In (A) protein A-purified anti-human GAA antibody was used. The levels of the precursor and the processed forms in WT fibers, but not in the KO fibers on ERT, are similar to those in whole tissue lysates. In (B) affinity-purified anti-human GAA antibody was used. This antibody recognized the 110-kDa administered rhGAA (0.05 ng), thus confirming its specificity. GAPDH was used as a loading control.

Discussion

We have demonstrated that in the GAA KO mice there is a progressive accumulation of autophagic material in multiple type II-rich muscles. The process appears to begin with the formation of a number of autophagosomes, usually in the core of the fiber. At a later stage, the same area becomes enlarged and filled with vesicles of the autophagic and endocytic pathways. Eventually, in older mice, the vesicular structures appear to be lost, leaving massive lakes of what we assume to be glycogen and the remnants of membranes. These data, therefore, challenge the current view that enlargement of glycogen-filled lysosomes leading to lysosomal rupture represents the *only* pathogenic mechanism of muscle damage.

The question remains as to what triggers the autophagy in type II KO fibers. Nutrient limitation is a powerful inducer of autophagy, and the autophagic response in skeletal muscle has been shown to be fiber-type specific; it is rapid and intense in type II-rich muscle, but moderate in type I-rich muscle [23]. We have previously suggested that a local nutritional stress in a segment of a fiber may be such a trigger [19]. Another condition that may induce autophagy is oxidative stress (reviewed in [24]). Based on experimental data showing reparative autophagocytosis in fibroblasts exposed to mild oxidative stress [25], Kiffin *et al*. hypothesized that moderate stress, affecting only a small number of lysosomes, may activate autophagy to sequester the leaking lysosomes [26]. A similar sequence of events could take place at the beginning stages of Pompe disease; the autophagy might be up-regulated to remove small damaged lysosomes. Our observation of autophagic vacuoles containing lysosomes without clear membrane boundaries in young KO mice supports such a possibility.

Regardless of whether oxidative stress contributes to the initial stage of the disease, its role is evident at the

doi:10.1016/j.ymthe.2006.08.009

later stages from the increased formation of lipofuscin. Nearly exclusive concentration of lipofuscin in the autophagic areas in the KO indicates that the process is disease related. Lipofuscin, an autofluorescent material composed of oxidatively modified molecules, normally accumulates in lysosomes of postmitotic cells during aging. However, an abnormal increase in lipofuscin is associated with oxidative stress [24,27,28]. Enhanced deposition of lipofuscin and large areas of centrally located cellular debris were observed by Hesselink *et al*. [29] in muscles of another mouse model of Pompe disease ($AGLU^{-/-}$) [30]; these inclusions most likely represent the autophagic area. The time course and the extent of the changes in the $AGLU^{-/-}$ mice, however, are quite different from those seen in the model reported here. One explanation for the discrepancy is that the disease is milder in $AGLU^{-/-}$ mice. A more likely explanation is different methods used to assess morphology.

The dysregulation of the autophagic pathway, which converges with the endocytic pathway at the late endosomes, may lead to the mistargeting of the endocytosed therapeutic enzyme. We addressed the issue by using a unique experimental system—analysis of endocytosis in live myofibers—which has been used only once before to characterize the endocytic compartments in normal fully differentiated rat myofibers from flexor digitorum brevis muscle [31]. We have presented here experimental evidence that the endocytosed therapeutic enzyme (and dextran) in the KO fibers accumulates along the length of the fibers, primarily in the vesicular compartments of the autophagic areas. Some of these compartments represent autophagosomes, late endosomes, intermediate autophagosomes, and possibly damaged nonfunctional lysosomes unable to degrade the autophagocytosed material. These structures, which include both intralysosomal (lipofuscin) and extralysosomal undigested material could be called biological garbage [24]. The recombinant enzyme, trapped in these areas, is wasted since it is diverted from glycogen-filled lysosomes in the rest of the fiber, but is unable to resolve the autophagic buildup [19], which continues to expand as the disease progresses.

Furthermore, processing of the rhGAA precursor to fully active mature forms seems to be altered in the diseased fibers. Cleavage of the precursor results in the activation of the enzyme, and it is the mature forms that are most active toward the natural substrate glycogen [10]. The conversion of the precursor to the 95-kDa intermediate most likely occurs in the late endocytic compartment. The subsequent conversion to the mature forms requires both proteases and glycosidases and is thought to occur in the lysosomes [10,11]. In the myofibers, processing of the 95-kDa intermediate to the 76-kDa mature form seems to be stalled, resulting in a shift in the ratio of these two forms toward the intermediate with a lower affinity for glycogen. Additionally, only a small part of the mature form detected in muscle biopsies after ERT actually reaches the myofibers. Thus, the mature GAA in nonmuscle components of a muscle biopsy contributes significantly to the overall level of enzyme detected after ERT. This finding should be considered when muscle biopsies are used to monitor the efficacy of ERT.

A number of factors make skeletal muscle a challenging target for ERT, among them are its sheer mass, the low density of CI-MPR [32], and the fact that the vast majority of the administered enzyme is delivered to the liver [17]. Type II fibers in the KO mice are at an even greater disadvantage since they have lower receptor density and lower levels of trafficking proteins compared to type I fibers [19]. Mistargeting of rhGAA in type II fibers exacerbates the problem. When the enzyme does reach the lysosomes, it seems to work well. However, the reversal of pathology in Pompe skeletal muscle requires more than clearance of lysosomal glycogen. Furthermore, assuming that similar autophagic changes occur in Pompe patients, the current therapy should be considered for presymptomatic late-onset patients, before autophagic buildup occurs.

Materials and Methods

A 110-kDa form of rhGAA was produced and purified from CHO cells (Genzyme Corp., Framingham, MA, USA). The following primary antibodies were used for immunostaining of fixed fibers: rabbit antiserum to bovine CI-MPR (1:15,000; a gift from Dr. Stuart Kornfeld, Washington University School of Medicine, St. Louis, MO, USA), rabbit anti-LC3 (microtubule-associated protein 1 light chain 3; 1:250; a gift from Dr. T. Ueno, Juntendo University School of Medicine, Juntendo, Japan), and rat anti-mouse LAMP1 (1:200; BD Pharmingen, San Diego, CA, USA). Protein A-purified and affinity-purified polyclonal rabbit anti-rhGAA antibodies were used for detection of GAA (Covance Research Products, Inc., Denver, PA). Mouse monoclonal anti-GAPDH antibody (1:5000; Abcam, Cambridge, MA, USA) served as a loading control. Alexa Fluor-conjugated antibodies (Molecular Probes, Eugene, OR, USA) were used as secondary antibodies for immunostaining and for Western analysis. LysoTracker Red DND-99 (Molecular Probes) was used for labeling acidic vesicles.

Isolation of fixed single muscle fibers and immunofluorescence microscopy. White G, TA, and EDL muscles were removed immediately after sacrifice from WT and KO [33] mice and pinned to Sylgaard-coated dishes for fixation with 2% paraformaldehyde in 0.1 M phosphate buffer for 1 h, followed by fixation in methanol (−20°C) for 6 min. Single fibers were obtained by manual teasing. Fibers were placed in a 24-well plate in blocking reagent (Vector Laboratories, Burlingame, CA, USA) for 1 h. The fibers were then permeabilized, incubated with primary antibody for overnight at 4°C, washed, incubated with secondary antibody for 2 h, washed again, and mounted in Vectashield (Vector Laboratories) on a glass slide. EDL and TA in mouse are a good source of fast-twitch type II fibers without any contribution of slow-twitch type I myofibers; white gastrocnemius muscle contains only ~1% type I fibers [34].

Isolation of live single muscle fibers. Single live myofibers were isolated from G, TA, and EDL muscles of 2- to 3-month-old WT and KO mice, as described [35] with modifications. Briefly, each dissected muscle group was placed in a Sylgaard plate containing DPBS. Muscles were pinned at resting length and cleaned of any extraneous material (the epimysium, fat, large tendons, and blood vessels) under a dissection microscope. Muscles were then digested in 0.2% (w/v) collagenase type 1 (Sigma, St. Louis, MO, USA) in Dulbecco's modified Eagle's medium (DMEM)

doi:10.1016/j.ymthe.2006.08.009

(GIBCO, Invitrogen, Carlsbad, CA, USA) for 1.5 h at 37°C in an atmosphere of 5% CO_2. Myofibers were isolated under a dissecting microscope by gentle trituration using a plastic pipette. Individual translucent myofibers were transferred to a fresh tissue culture dish that contained warmed DMEM. After three or four serial transfers myofibers were cultured in the uptake medium [Ham's F-12 medium (GIBCO, Invitrogen), 10% FBS, and 3 mM Pipes, pH 6.7] [36]. Our attempt to isolate live muscle fibers from 24-month-old KO mice failed, presumably because the fibers were extremely fragile.

Protein labeling and GAA enzyme activity. rhGAA was labeled and purified using the Alexa Fluor 546 Protein Labeling Kit (Molecular Probes) according to the manufacturer's instructions. The degree of labeling was 2.9–4.4 mol dye/mol protein. The amount of free dye in the labeled protein fraction was determined by TLC. GAA activity of the labeled enzyme, measured as described [37], was 50–80% of that of the unlabeled rhGAA.

Endocytosis in live cultured muscle fibers. Myofibers were cultured in chambered coverglasses overnight in the presence of either Alexa Fluor 546-labeled rhGAA (200 nM) or Alexa Fluor 546-conjugated dextran (2 mg/ml; Molecular Probes) at 37°C in an atmosphere of 5% CO_2. The fibers were then washed with DMEM and analyzed by confocal microscopy (Zeiss LSM 510 META). In a separate series of experiments, the fibers were incubated overnight with equal fluorescent units of the dye alone. In some experiments the fibers were preincubated with 5 mM M6P (Sigma) or a 100-fold excess of rhGAA (cold) for 2 h prior to incubation with labeled rhGAA (70 nM).

Spectral unmixing analysis. The muscle fibers, and in particular the autophagic area, have considerable amounts of autofluorescent signal; they will fluoresce even when not labeled with external sources of fluorophores. In samples (fibers) labeled with Alexa Fluor 546-rhGAA, the fluorophore and the autofluorescent compounds both emit in the same range. Traditional filter-based technology is unable to separate these overlapping spectra, as only the number of photons per pixel is detected and not the wavelength of the emission. To discriminate autofluorescence signal from the Alexa Fluor 546 signal (which represents the location of GAA), we employed a postimage spectral unmixing analysis. Autofluorescence and Alexa 546 emission signals were separated using the LSM 510 META detector and the linear unmixing software provided. Images of unlabeled myofibers and Alexa Fluor 546-rhGAA (a fiber-free solution) were collected using a 543-nm laser line and the emission range set from 582 to 700 nm. The reference spectra (emission fingerprints) from the unlabeled fibers and Alexa Fluor 546-rhGAA are unique in shape. The images from labeled and unlabeled fibers were collected using identical optical paths and the LSM 510 META detector. Spectral unmixing compares the emission profile of a sample to that of the stored reference spectra and displays the contributions of Alexa Fluor 546 and autofluorescence separately. This method allowed us to demonstrate the location of the endocytosed Alexa Fluor 546-rhGAA in fibers with high autofluorescence. A similar procedure was used for the experiments with labeled dextran.

Western blot of muscle tissues and muscle fibers. Whole muscle tissues were removed from 2- to 3-month-old KO mice that received a single intravenous injection of rhGAA (50 mg/kg). In some experiments multiple injections of rhGAA were performed (30 mg/kg twice/week × 16 injections) in tolerant KO mice [38]. Mice were sacrificed 24 h after the last injection. Each hind limb was used to prepare protein lysates from whole muscle tissues or from fibers. The lysates were prepared in RIPA buffer and separated by SDS–PAGE (50 μg protein/lane) as described [18]. Blots were scanned on an infrared imager (Li-COR Biosciences, Lincoln, NE, USA).

Animal care and experiments were conducted in accordance with the NIH *Guide for the Care and Use of Laboratory Animals*.

ACKNOWLEDGMENTS

This research was supported by the Intramural Research Program of the National Institute of Arthritis and Musculoskeletal and Skin Diseases of the National Institutes of Health. We are grateful to Karen Lee (Genzyme Corp., Framingham, MA, USA) for providing some of the batches of labeled rhGAA. We thank Lyuben Marekov (NIAMS, NIH) for his help in labeling rhGAA and Stephanie Carroll (NHLBI, NIH) for sharing her knowledge of isolation of live muscle fibers.

RECEIVED FOR PUBLICATION MAY 24, 2006; REVISED AUGUST 6, 2006; ACCEPTED AUGUST 17, 2006.

REFERENCES

1. Sly, W. S. (2004). Enzyme replacement therapy for lysosomal storage disorders: successful transition from concept to clinical practice. *Mol. Med.* **101:** 100–104.
2. Hirschhorn, R., and Reuser, A. J. (2001). Glycogen storage disease type II: acid alpha-glucosidase (acid maltase) deficiency. In: *The Metabolic and Molecular Basis of Inherited Disease* (C. R. Scriver, A. L. Beaudet, W. S. Sly, D. Valle, Eds.), pp. 3389–3420. McGraw–Hill, New York.
3. Van den Hout, *et al.* (2003). The natural course of infantile Pompe's disease: 20 original cases compared with 133 cases from the literature. *Pediatrics* **112:** 332–340.
4. Kishnani, P. S., Hwu, W. L., Mandel, H., Nicolino, M., Yong, F., and Corzo, D. (2006). A retrospective, multinational, multicenter study on the natural history of infantile-onset Pompe disease. *J. Pediatr.* **148:** 671–676.
5. Hagemans, M. L., *et al.* (2005). Clinical manifestation and natural course of late-onset Pompe's disease in 54 Dutch patients. *Brain* **128:** 671–677.
6. Hagemans, M. L., Winkel, L. P., Hop, W. C., Reuser, A. J., Van Doorn, P. A., and Van der Ploeg, A. T. (2005). Disease severity in children and adults with Pompe disease related to age and disease duration. *Neurology* **64:** 2139–2141.
7. Kornfeld, S. (1992). Structure and function of the mannose 6-phosphate/insulin-like growth factor II receptors. *Annu. Rev. Biochem.* **61:** 307–330.
8. Kornfeld, S., and Mellman, I. (1989). The biogenesis of lysosomes. *Annu. Rev. Cell Biol.* **5:** 483–525.
9. Ghosh, P., Dahms, N. M., and Kornfeld, S. (2003). Mannose 6-phosphate receptors: new twists in the tail. *Nat. Rev. Mol. Cell Biol.* **4:** 202–212.
10. Wisselaar, H. A., Kroos, M. A., Hermans, M. M., van Beeumen, J., and Reuser, A. J. (1993). Structural and functional changes of lysosomal acid alpha-glucosidase during intracellular transport and maturation. *J. Biol. Chem.* **268:** 2223–2231.
11. Moreland, R. J., *et al.* (2005). Lysosomal acid alpha-glucosidase consists of four different peptides processed from a single chain precursor. *J. Biol. Chem.* **280:** 6780–6791.
12. Amalfitano, A., *et al.* (2001). Recombinant human acid alpha-glucosidase enzyme therapy for infantile glycogen storage disease type II: results of a phase I/II clinical trial. *Genet. Med.* **3:** 132–138.
13. Van den Hout, J. M., *et al.* (2004). Long-term intravenous treatment of Pompe disease with recombinant human alpha-glucosidase from milk. *Pediatrics* **113:** e448–e457.
14. Winkel, L. P., *et al.* (2003). Morphological changes in muscle tissue of patients with infantile Pompe's disease receiving enzyme replacement therapy. *Muscle Nerve* **27:** 743–751.
15. Winkel, L. P., *et al.* (2004). Enzyme replacement therapy in late-onset Pompe's disease: a three-year follow-up. *Ann. Neurol.* **55:** 495–502.
16. Klinge, L., *et al.* (2005). Safety and efficacy of recombinant acid alpha-glucosidase (rhGAA) in patients with classical infantile Pompe disease: results of a phase II clinical trial. *Neuromuscul. Disord.* **15:** 24–31.
17. Raben, N., *et al.* (2003). Enzyme replacement therapy in the mouse model of Pompe disease. *Mol. Genet. Metab.* **80:** 159–169.
18. Raben, N., *et al.* (2005). Replacing acid alpha-glucosidase in Pompe disease: recombinant and transgenic enzymes are equipotent, but neither completely clears glycogen from type II muscle fibers. *Mol. Ther.* **11:** 48–56.
19. Fukuda, T., *et al.* (2006). Dysfunction of endocytic and autophagic pathways in a lysosomal storage disease. *Ann. Neurol.* **59:** 700–708.
20. Klionsky, D. J., and Emr, S. D. (2000). Autophagy as a regulated pathway of cellular degradation. *Science* **290:** 1717–1721.
21. Yorimitsu, T., and Klionsky, D. J. (2005). Autophagy: molecular machinery for self-eating. *Cell Death Differ.* **12**(Suppl. 2)**:** 1542–1552.
22. Yoshimori, T. (2004). Autophagy: a regulated bulk degradation process inside cells. *Biochem. Biophys. Res. Commun.* **313:** 453–458.
23. Mizushima, N., Yamamoto, A., Matsui, M., Yoshimori, T., and Ohsumi, Y. (2004). In vivo analysis of autophagy in response to nutrient starvation using transgenic mice expressing a fluorescent autophagosome marker. *Mol. Biol. Cell* **15:** 1101–1111.
24. Terman, A., and Brunk, U. T. (2006). Oxidative stress, accumulation of biological 'garbage', and aging. *Antioxid. Redox Signaling* **8:** 197–204.
25. Brunk, U. T., Dalen, H., Roberg, K., and Hellquist, H. B. (1997). Photo-oxidative disruption of lysosomal membranes causes apoptosis of cultured human fibroblasts. *Free Radic. Biol. Med.* **23:** 616–626.
26. Kiffin, R., Bandyopadhyay, U., and Cuervo, A. M. (2006). Oxidative stress and autophagy. *Antioxid. Redox Signaling* **8:** 152–162.
27. Terman, A., and Brunk, U. T. (2004). Lipofuscin. *Int. J. Biochem. Cell Biol.* **36:** 1400–1404.
28. Brunk, U. T., and Terman, A. (2002). Lipofuscin: mechanisms of age-related

doi:10.1016/j.ymthe.2006.08.009

accumulation and influence on cell function. *Free Radic. Biol. Med.* **33:** 611–619.

29. Hesselink, R. P., Schaart, G., Wagenmakers, A. J., Drost, M. R., and van der Vusse, G. J. (2005). Age-related morphological changes in skeletal muscle cells of acid alpha-glucosidase knockout mice. *Muscle Nerve* **33:** 505–513.

30. Bijvoet, A. G., *et al.* (1998). Generalized glycogen storage and cardiomegaly in a knockout mouse model of Pompe disease. *Hum. Mol. Genet.* **7:** 53–62.

31. Kaisto, T., Rahkila, P., Marjomaki, V., Parton, R. G., and Metsikko, K. (1999). Endocytosis in skeletal muscle fibers. *Exp. Cell Res.* **253:** 551–560.

32. Funk, B., Kessler, U., Eisenmenger, W., Hansmann, A., Kolb, H. J., and Kiess, W. (1992). Expression of the insulin-like growth factor-II/mannose-6-phosphate receptor in multiple human tissues during fetal life and early infancy. *J. Clin. Endocrinol. Metab.* **75:** 424–431.

33. Raben, N., *et al.* (1998). Targeted disruption of the acid alpha-glucosidase gene in mice causes an illness with critical features of both infantile and adult human glycogen storage disease type II. *J. Biol. Chem.* **273:** 19086–19092.

34. Burkholder, T. J., Fingado, B., Baron, S., and Lieber, R. L. (1994). Relationship between muscle fiber types and sizes and muscle architectural properties in the mouse hindlimb. *J. Morphol.* **221:** 177–190.

35. Rosenblatt, J. D., Lunt, A. I., Parry, D. J., and Partridge, T. A. (1995). Culturing satellite cells from living single muscle fiber explants. *In Vitro Cell Dev. Biol. Anim.* **31:** 773–779.

36. Reuser, A. J., *et al.* (1984). Uptake and stability of human and bovine acid alpha-glucosidase in cultured fibroblasts and skeletal muscle cells from glycogenosis type II patients. *Exp. Cell Res.* **155:** 178–189.

37. Hermans, M. M., Kroos, M. A., van Beeumen, J., Oostra, B. A., and Reuser, A. J. (1991). Human lysosomal alpha-glucosidase: characterization of the catalytic site. *J. Biol. Chem.* **266:** 13507–13512.

38. Raben, N., *et al.* (2003). Induction of tolerance to a recombinant human enzyme, acid alpha-glucosidase, in enzyme deficient knockout mice. *Transgenic Res.* **12:** 171–178.